Efficient nickel(II) immobilized on EDTA-modified $Fe_3O_4@SiO_2$ nanospheres as a novel nanocatalyst for amination of heteroaryl carbamates and sulfamates through the cleavage of C-O bond

Iman Dindarloo Inaloo[a,*], Sahar Majnooni[b], Hassan Eslahi[a], Mohsen Esmaeilpour[a]

[a] *Chemistry Department, College of Science, Shiraz University, Shiraz 71454, Iran*
[b] *Department of Chemistry, University of Isfahan, Isfahan 81746-73441, Iran*

ARTICLE INFO

ABSTRACT

In this report, there was immobilized Nickel(II) on EDTA-modified $Fe_3O_4@SiO_2$ nanospheres and catalytic activity of which was described in the arylation reaction of nitrogen nucleophiles *via* carbon-oxygen bond cleavage of (hetero)aryl carbamates and sulfamates. This protocol was applied to various nitrogen nucleophiles such as amines, anilines and *N*-heterocyclic compounds (pyrroles, indoles and imidazoles) in good to excellent yields. This reaction was promoted without the use of any external ligands under simple and mild conditions. The synthesized catalyst was well characterized by FT-IR, XRD, TEM, FE-SEM, TGA, DLS,XPS, VSM, EDX, ICP and nitrogen adsorption-desorption isotherm analysis. The recycling studies revealed that the catalyst could be easily recovered by used the external magnetic field and directly reused for at least 7 times without the significant decrease in its catalytic activity.

1. Introduction

Nitrogen–carbon bond formations have become efficient and useful processes for the preparation of various functionalized natural and artificial products [1–3]. Due to our growing requirement for the synthesis of such classes of compounds that have widespread applications in pharmaceutical and agricultural industries [1–3], many efforts have been carried out to provide effective and efficient C−N formation methodologies for finding new compounds [4–7]. In1983, Toshihiko Migita reported the synthesis of anilines with cross-coupling of tin amides and aryl bromides in the presence of palladium for the first time [8] and then, these catalytic amination reactions of aryl halides (I, Br, Cl, F) have been attracted many attentions as the most common and powerful systems for cross-coupling reactions [9,10]. Although these reactions have been gotten significant advancements over the last decade, the high cost and toxicity of aryl halides preparation and the stoichiometric waste of halide generated from these reactions limit their applications in both academic research and industrial productions, especially in the drug design process [11,12].

Thus, the designing and development of eco-friendly, facile and efficient methods for the direct *N*-arylation reactions through transition-metal catalyzed approaches were highly desired and beneficial in recent decades [13]. One of the new strategies that attracted a lot of

attention is the extensive effort for finding suitable and green alternatives for aryl halides due to the disadvantages were listed above [14]. In this regard, phenolic derivatives such as methyl ethers [15–17], pivalate esters [18,19], mesylate [20–22], tosylates [23,24], phosphate [25,26], sulfamates [27–29], carbonates [30–32] and carbamates [33–35] are the most common groups that have been received considerable attention. Although the phenolic derivatives as electrophiles are less reactive than aryl halides in the catalytic amination reactions, the use of these compounds have several extraordinary advantages including the wide scope, availability from natural sources and unconventional synthetic strategies, high stability and safety [36–41].

In continuous research to find the effective, eco-friendly and simple methodology, different transition-metals including Cu [42–45], Ni [46–50], Fe [51,52], Mn [53–55] and Co [56,57] have been investigated. However, most studies have been focused on copper-based complexes as catalysts at the beginning of the twenty-first century [42–45]. Recently, nickel has been widely applied as the catalyst for designing the new methodology in organic synthesis as a non-toxic metal with relatively high natural abundance and desirable reactivity properties [58–63]. In this field, Bolm reported the amination reaction of tosylates in the presence of Ni catalyst to explore the cross-coupling reactions of phenolic derivatives [64]. Subsequently, many efforts have also been devoted towards the finding of the effective approach of C−N
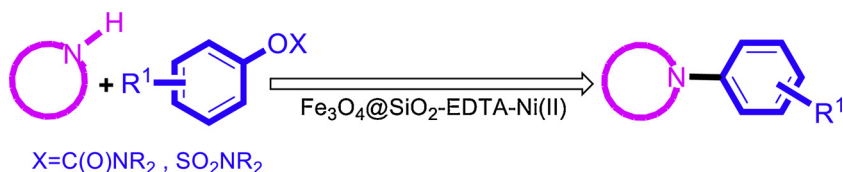
---

* Corresponding author.
E-mail address: iman.dindarlooinaloo@gmail.com (I. Dindarloo Inaloo).

Scheme 1. *N*-Arylation of nitrogen-containing compounds with nickel-based catalysis *via* C−O bond activation of phenol derivatives.
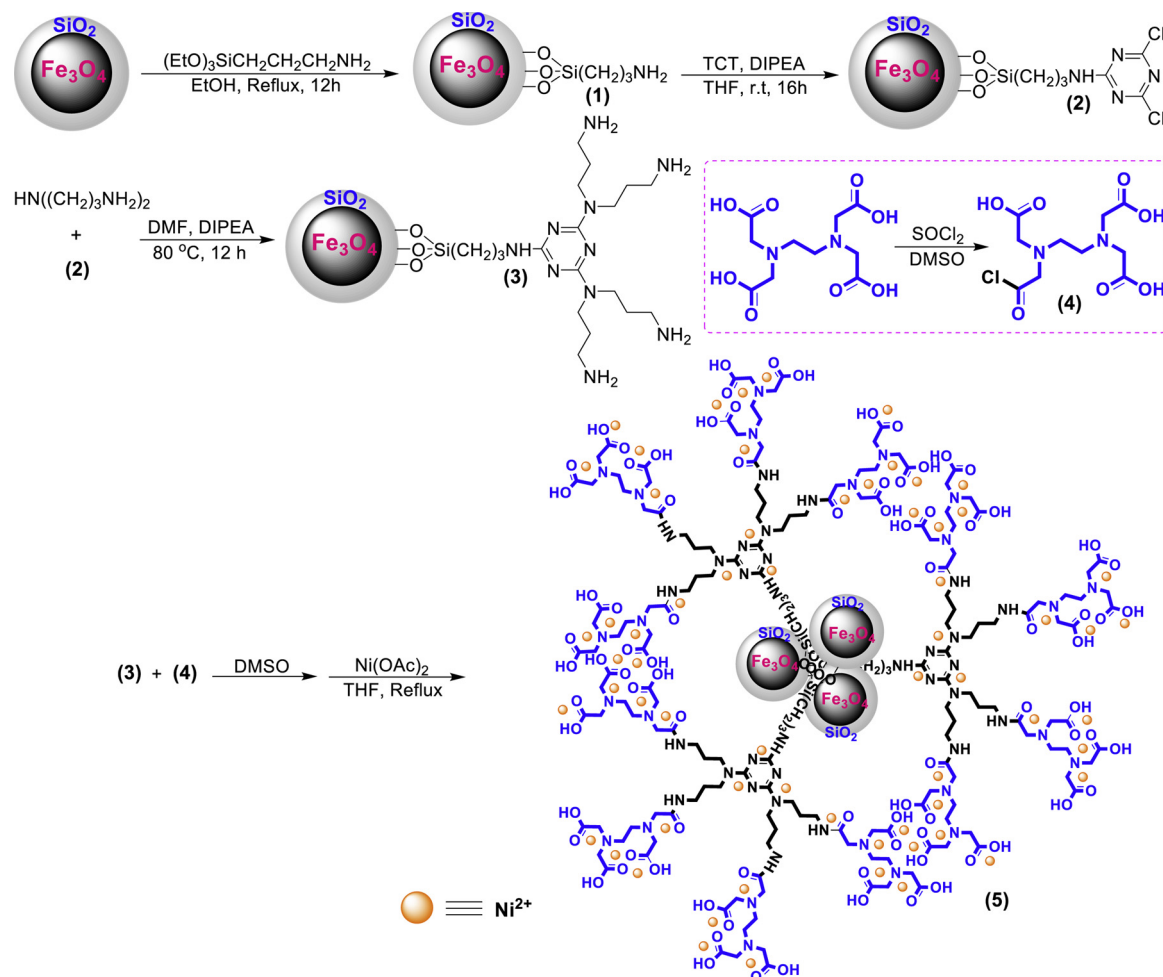
Scheme 2. Preparation of the Fe₃O₄@SiO₂-EDTA-Ni (II) nanocatalyst.

couplings using the nickel catalysts [65–68]. These studies and investigations have led us to construct a lot of nickel catalysts to make these reactions so effective and notably efficient [69–72].

These reactions have amazing and fantastic results; however, most of them suffer from some limitations such as using high catalyst amounts in addition to the presence of some expensive and unrecyclable external ligands including *N*-heterocyclic carbine or phosphine ligands. As a result, the development of novel and effective Ni-based C−N bond formation methods is of great importance [65–72]. On the other hand, the synthesis of the economical catalytic system that can be easily recovered and reused several times without losing efficiency has been intensively investigated over the last years due to environmental and conservation points of view [73–76]. Magnetic separation is a green and eco-friendly process to recover magnetic heterogeneous catalysts without filtering or centrifuging [77–79]. Therefore, the preparation of recoverable magnetic catalysts bearing magnetic materials has been widely investigated [80–82]. Among all magnetic materials, iron oxides are usually being applied as the popular magnetically material because of their special properties such as non-toxicity, low-cost preparation, amenable to functionalization and easy to handle [83,84].

Superparamagnetic Fe₃O₄ cores at the centre of the initial silica colloids and the obtained catalysts have recently been received significant attention due to their high stability and efficiency, simple work-up, efficient recovery and good reusability [85–88].

In continuation of our interests in the synthesis and using efficient superparamagnetic nanocatalysts in various interesting and important reaction [89–92], we reported the synthesis, characterizations and employment of nickel(II) nanoparticles immobilized on EDTA-modified Fe₃O₄@SiO₂nanospheres (Fe₃O₄@SiO₂-EDTA-Ni(II)) as reusable and efficient catalyst for the *N*-arylation of nitrogen-containing compounds with a library of amines, anilines, indoles and imidazoles *via* C−O bond activation of aryl carbamates and sulfamates as phenol derivatives under mild conditions (Scheme 1).

2. Materials and methods

2.1. Chemicals and instrumentation

All chemicals were purchased from the Flucka, Merck and Aldrich Chemical Companies with high purity. The products were characterized
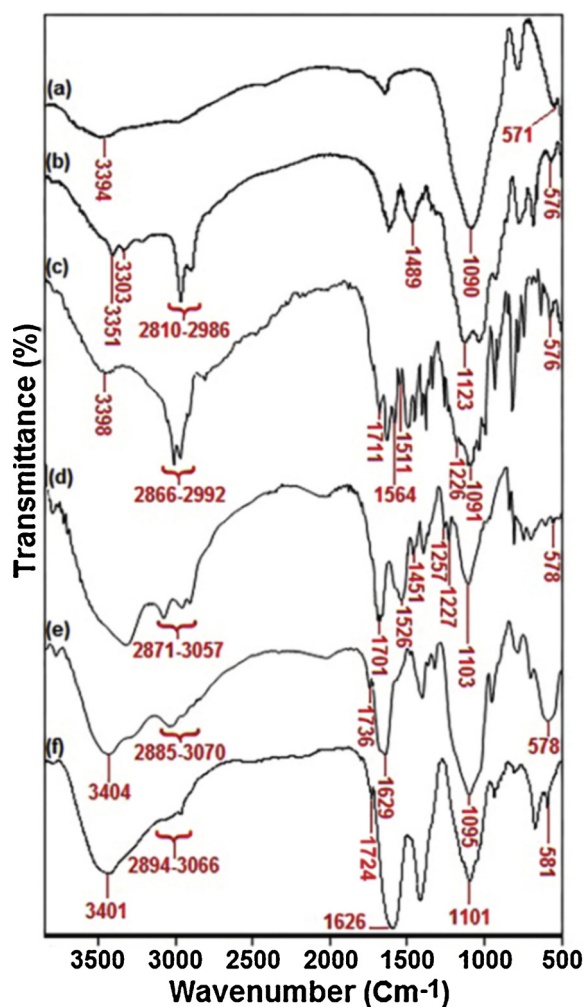
Fig. 1. FT-IR spectra of (a) $Fe_3O_4@SiO_2$, (b) $Fe_3O_4@SiO_2$-NH$_2$, (c) $Fe_3O_4@SiO_2$-TCT, (d) $Fe_3O_4@SiO_2$-TCT-NH$_2$, (e) $Fe_3O_4@SiO_2$-EDTA and (f) $Fe_3O_4@SiO_2$-EDTA-Ni(II) NPs.

Fig. 2. XRD diffraction pattern of (a) Fe_3O_4, (b) $Fe_3O_4@SiO_2$ and (c) $Fe_3O_4@$SiO$_2$-EDTA-Ni(II) NPs.

and analyzed by comparison of their spectral and physical data such as melting point, FT-IR, NMR, MS and CHNS with available literature data. ^{1}H and ^{13}C NMR spectra were recorded with Bruker Avance DPX250 MHz instruments with Me$_4$Si or solvent resonance as the internal standard. Fourier transforms infrared (FTIR) spectra were obtained using a Shimadzu FT-IR 8300 spectrophotometer. Powder X-ray diffraction (XRD) patterns were recorded in a Bruker AXS D8-advance X-ray diffract to the meter using Cu Kα radiation (λ = 1.5418). Transmission electron microscopy (TEM) images were taken on a Philips EM208 microscope with an accelerating voltage of 100 kV. The hydrodynamic size of the particles was measured by dynamic light scattering (DLS) techniques, using a HORIBA-LB550 particle size analyzer. The surface composition was investigated using an X-ray photoelectron spectroscopy (XPS) on XR3E2 (VG Microtech) spectrometer using Mg and Al twin anode X-ray gun with the multichannel detector and a hemispherical analyzer with a resolution of 1.0 eV. The nickel loading and leaching test were carried out with an inductively coupled plasma (ICP) analyzer (Varian, vista-pro). Determination of the purity of the substrate and monitoring of the reactions was accomplished by thin-layer chromatography (TLC) on a silica-gel polygram SILG/UV 254 plates.
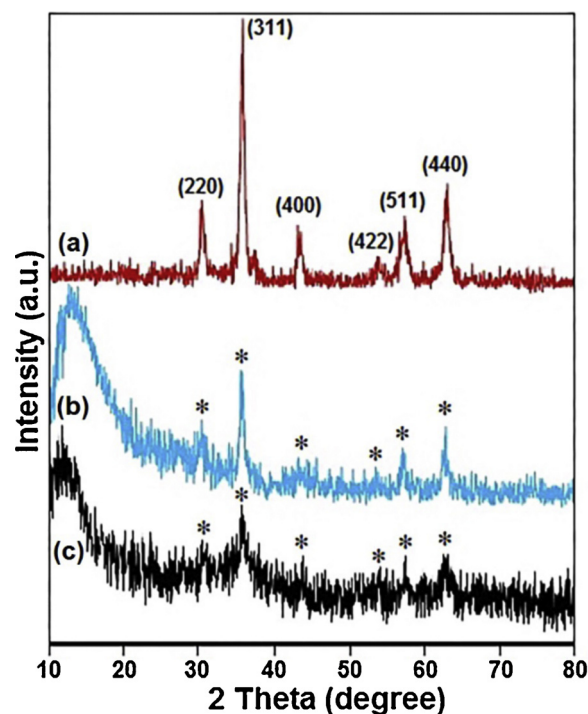
2.2. Materials synthesis

2.2.1. Preparation of Fe_3O_4 NPs

Considering the reported method [89–92], 0.9 g of FeCl$_2$·4H$_2$O 4.5 mmol), 1.3 g of FeCl$_3$·6H$_2$O (4.8 mmol) and 1 g of surfactant poly (vinyl alcohol) (PVA 15,000) were dissolved in 40 mL deionized water. The mixture was vigorously stirred at 80 °C for 30 min and then, hexamethylenetetramine (1.0 mmol) was slowly added to the solution to adjust the pH of the solution (~ 10.0). After stirring the mixture for 2 h, the black magnetite was finally collected by an external magnetic field, rinsed with ethanol several times and dried under vacuum at 80 °C for 10 h.

2.2.2. Preparation of $Fe_3O_4@SiO_2$ NPs [89–92]

The silica coating over the Fe_3O_4 nanoparticles was achieved *via* a well-known Stober method in which 50 mL solvent bearing ethanol/deionized water (10:1) was applied to disperse 0.5 g of synthesized Fe_3O_4 nanoparticles using ultrasound irradiation followed by the addition of 0.2 mL of tetraethoxysilane (TEOS). During the next step, 5 mL of NaOH (10 wt%,) solution was added to the mixture at room temperature and it was stirred for 30 min. The resulting $Fe_3O_4@SiO_2$ MNPs were collected by an external magnet, washed with distilled water and ethanol, and dried in a vacuum oven at 80 °C for 10 h.

2.2.3. Synthesis of $Fe_3O_4@SiO_2$-NH$_2$NPs [89–92]

The functionalization of prepared core-shell was started with adding 0.25 mL of 3-aminopropyl(triethoxy)silane (1 mmol) to a suspension of $Fe_3O_4@SiO_2$(1 g) in 10 mL of ethanol and stirring for 12 h under the reflux conditions. Then, after cooling the crude to room temperature, the obtained brown precipitate was collected with an external magnet washed with water and ethanol (1:1) and dried under vacuum at 80 °C.

2.2.4. Synthesis of $Fe_3O_4@SiO_2$-TCT NPs

1 g of $Fe_3O_4@SiO_2$-NH$_2$ NPs was dispersed in 10 mL of THF having dissolved 1 mmol (0.185 g) of cyanuric chloride (TCT) and 1 mmol (0.17 mL) of diisopropylethylamine (DIPEA). The crude was stirred for 16 h at room temperature and then, $Fe_3O_4@SiO_2$-TCT NPs were

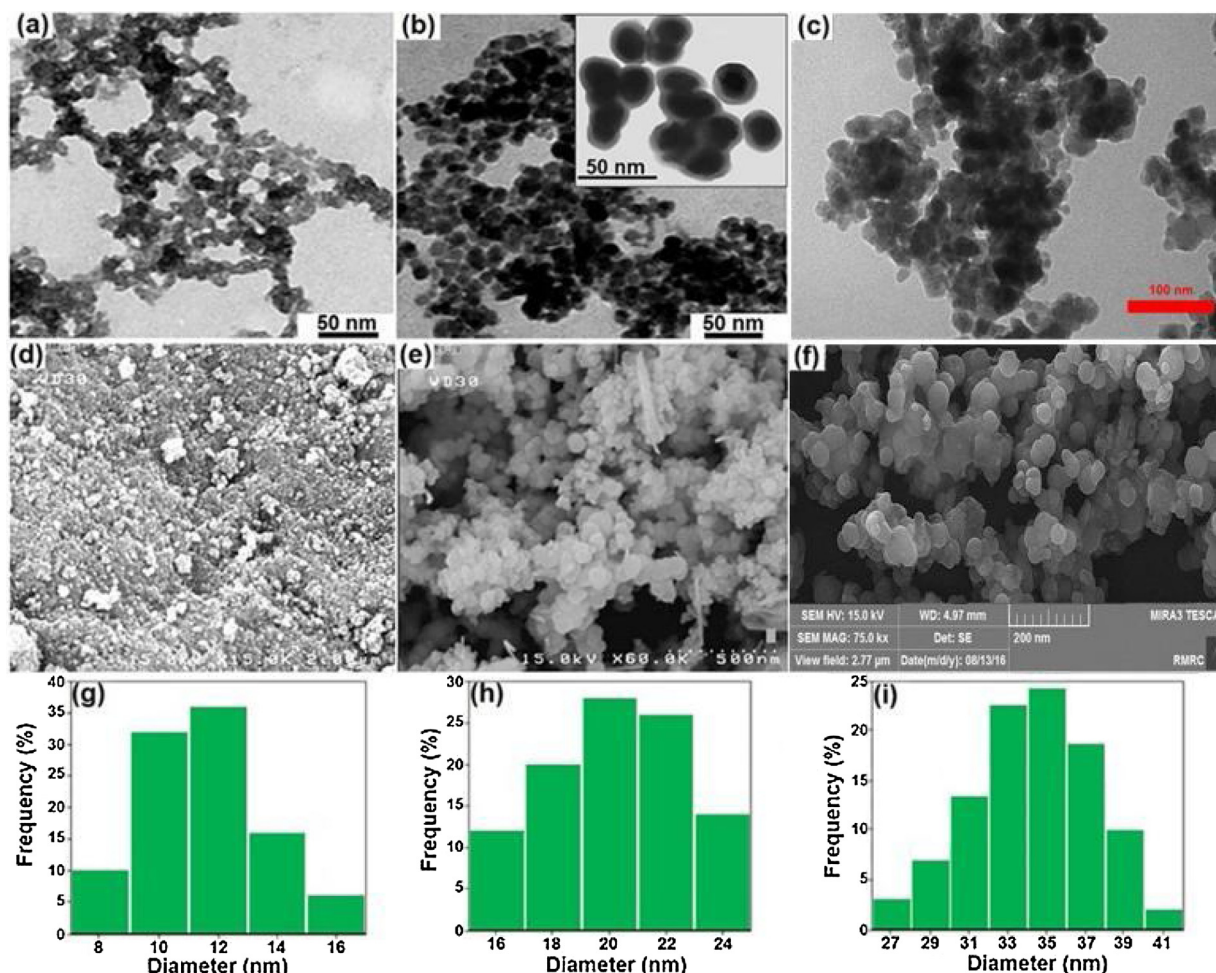**Fig. 3.** TEM images of (a) Fe₃O₄, (b) Fe₃O₄@SiO₂, and (c) Fe₃O₄@SiO₂-EDTA-Ni(II); FE-SEM images of (d) Fe₃O₄, (e) Fe₃O₄@SiO₂, and (f) Fe₃O₄@SiO₂-EDTA-Ni(II) and the size distributions of (g) Fe₃O₄, (h) Fe₃O₄@SiO₂, and (i) Fe₃O₄@SiO₂-EDTA-Ni(II) NPs, respectively.

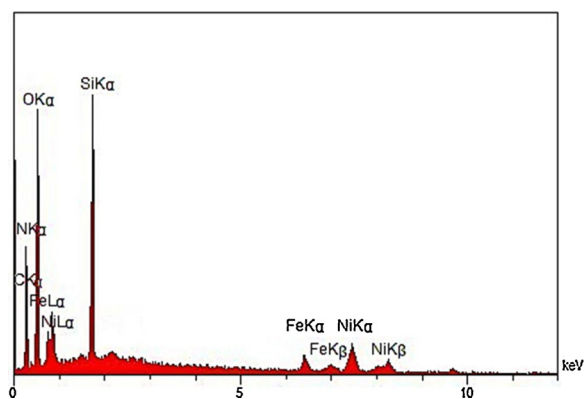**Fig. 4.** EDX spectrum of Fe₃O₄@SiO₂-EDTA-Ni(II)NPs.

collected by a magnet, washed with distilled water and ethanol (1:1) solution three times and dried at 60 °C.

2.2.5. Synthesis of Fe₃O₄@SiO₂-TCT-NH₂ NPs

At the first, cyanuric chloride immobilized Fe₃O₄@SiO₂-NH₂NPs (1.0 g) was dispersed in 5 mL of DMF and 0.25 mL of bis(3-amino-propyl)amine (2 mmol) and DIPEA (2 mmol, 0.35 mL) were added to the mixture. After stirring at 80 °C for 12 h, the precipitate (Fe₃O₄@SiO₂-TCT-NH₂) was magnetically collected from the solution, washed with water and ethanol several times and dried at 70 °C for 4 h.

2.2.6. Synthesis of Fe₃O₄@SiO₂-TCT-EDTANPs

The solution of thionyl chloride (SOCl₂) (2 mmol) in DMSO (5 mL) was added dropwise into the solution of EDTA (2 mmol) in DMSO (15 mL) and the obtained mixture was vigorously stirred for 3 h. Then, Fe₃O₄@SiO₂-TCT-NH₂ (1.5 g) was added to the mixture at room temperature. After 2 h, the magnetic moiety was separated by an external magnet, washed with an aqueous solution of Na₂CO₃ (0.1 mol L⁻¹) and subsequently, with acetone. Finally, they were dried at 60 °C to obtain Fe₃O₄@SiO₂-EDTA NPs.

2.2.7. Synthesis of Fe₃O₄@SiO₂-TCT-EDTA-Ni(II)NPs

In this step, 1.5 g of as-prepared Fe₃O₄@SiO₂-EDTA and 1 g of nickel (II) acetate tetrahydrate (4 mmol) were dispersed in 10 mL of THF by ultrasonication and stirred for 4 h under the reflux conditions. Fe₃O₄@SiO₂-EDTA-Ni NPs were collected by a magnet, washed with water and ethanol several times and dried at 60 °C overnight.

2.2.8. General procedure for the N-arylation of nitrogen-containing compounds with C–O activation of aryl carbamate and/or aryl sulfamate

Aryl carbamate and/or aryl sulfamate (1.0 mmol), nitrogen-containing compounds (1.0 mmol), sodium *tert*-butoxide (2.0 mmol), Fe₃O₄@SiO₂-EDTA-Ni(II) NPs (0.018 g, 1 mol %) and ethylene glycol (3.0 mL) were added into a round-bottomed flask and stirred at 100 °C for 12 h under the inert nitrogen atmosphere. The reaction progress was monitored by TLC using petroleum ether/ethyl acetate and/or GC (argon in 5.0 grades or 99.999% purity as carrier gas and PEG as stationary phase). After the completion of the reaction, the reaction
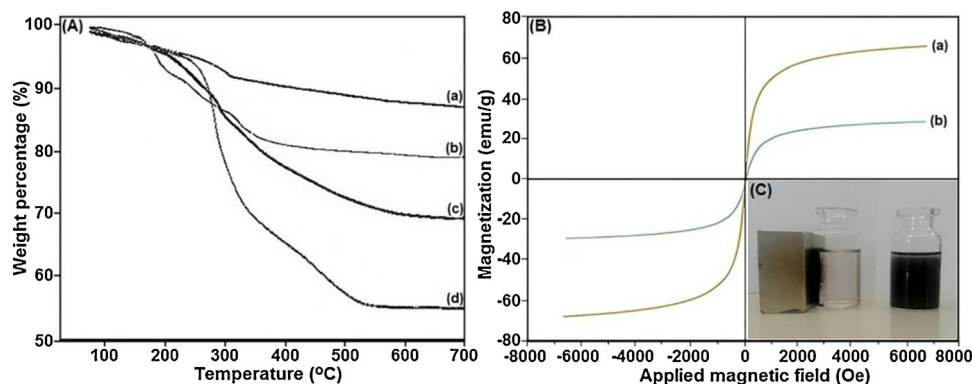
Fig. 5. TGA spectrum of (a) $Fe_3O_4@SiO_2-NH_2$, (b) $Fe_3O_4@SiO_2-TCT$, (c) $Fe_3O_4@SiO_2-TCT-NH_2$ and (d) $Fe_3O_4@SiO_2-EDTA-Ni(II)$ NPs; andMagnetic hysteresis loops of (a) Fe_3O_4 and (b) $Fe_3O_4@SiO_2-EDTA-Ni(II)$ NPs.

Table 1
Selected properties of Fe_3O_4, $Fe_3O_4@SiO_2$ and $Fe_3O_4@SiO_2-EDTA-Ni(II)$ NPs.

Sample	Fe_3O_4 crystal structure	Specific surface area (m^2/g)[a]	Magnetite particle size (nm)[b]
Fe_3O_4	Cubic spinel	480	11.33
$Fe_3O_4@SiO_2$	Cubic spinel	430.3	12.64
$Fe_3O_4@SiO_2-EDTA-Ni(II)$	Cubic spinel	371.6	14.97

[a] Calculated by the BJH method.
[b] Calculated by the Scherrer equation based on powder X-ray diffraction (XRD) patterns.

Table 2
TGA and elemental analysis for $Fe_3O_4@SiO_2-NH_2$, $Fe_3O_4@SiO_2-TCT$, $Fe_3O_4@SiO_2-TCT-NH_2$ and $Fe_3O_4@SiO_2-EDTA-Ni(II)$ NPs.

Sample		C (%)	H (%)	N (%)	Total (%)[a]
$Fe_3O_4@SiO_2-NH_2$	TGA (wt%)	6.746	1.501	2.627	10.874
	EA (wt%)	6.614	1.475	2.532	10.621
$Fe_3O_4@SiO_2-TCT$	TGA (wt%)	7.377	0.717	5.736	13.830
	EA (wt%)	7.468	0.750	5.627	13.845
$Fe_3O_4@SiO_2-TCT-NH_2$	TGA (wt%)	16.172	2.918	10.564	29.654
	EA (wt%)	15.946	2.871	10.377	29.194
$Fe_3O_4@SiO_2-EDTA-Ni(II)$	TGA (wt%)	22.821	2.853	9.112	34.786
	EA (wt%)	21.611	2.871	9.232	33.714

[a] Total (%) = C (%) + H (%) + N (%).

mixture was cooled to room temperature and the nanocatalysts separated from the mixture with an external magnetic field. Then, water (10 mL) was added and the crude mixture was subsequently extracted with ethyl acetate (3 × 10 mL). The organic phases were dried over anhydrous $MgSO_4$ and the crude product was obtained after removing the ethereal solution by a rotary evaporator. The product was finally purified by column chromatography on silica gel using petroleum ether/ethyl acetate (10:2) as the solvent or recrystallized.
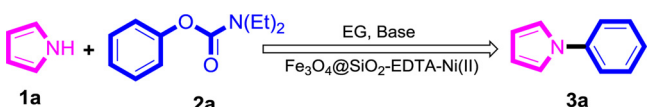
3. Results and discussion

The prepared $Fe_3O_4@SiO_2-EDTA-Ni(II)$ NPs were synthesized *via* the multistep procedure (Scheme 2) and well-characterized by the following instrumental techniques: FT-IR, XRD, TEM, FE-SEM, DLS, EDX, XPS, TGA, VSM, BET, ICP and elemental analysis.

The successful functionalization of the MNPs surface was confirmed by examination of the FTIR spectra. Fig. 1 shows the FT-IR spectra of the $Fe_3O_4@SiO_2$, $Fe_3O_4@SiO_2-NH_2$, $Fe_3O_4@SiO_2-TCT$, $Fe_3O_4@SiO_2-TCT-NH_2$, $Fe_3O_4@SiO_2-EDTA$ and $Fe_3O_4@SiO_2-EDTA-Ni(II)$ NPs. All spectra shows broad bands at around $3400 \, cm^{-1}$ and $580 \, cm^{-1}$, which are the characteristic of stretching bands of O−H and Fe–O bonds,

respectively. In the case of $Fe_3O_4@SiO_2$ NPs, the sharp band at $1090 \, cm^{-1}$ corresponds to overlapped Si–O–Si symmetric and asymmetric stretching vibrations (Fig. 1a). The characteristic absorption bands at 2810–2986, 1489, 1123, and $576 \, cm^{-1}$ correspond to the C–H (stretching vibration), CH_2 (bending), Si–O–Si (stretching vibration), and Fe–O (stretching vibration), respectively, proving the existence of 3-aminopropyl(triethoxy)silanefunctional groups on the surface of $Fe_3O_4@SiO_2$ NPs. Furthermore, the peaks at about $3300 - 3400 \, cm^{-1}$ can be ascribed to NH_2 stretching vibrations (Fig. 1b). In the spectrum of $Fe_3O_4@SiO_2-TCT$ NPs, the characteristic adsorptions at 1711, 1564 and $1511 \, cm^{-1}$are attributed to C=N stretching vibrations (Fig. 1c). The peak at $1091 \, cm^{-1}$ was attributed to the C–Cl groups of cyanuric chloride, which is overlapped by the stretching vibration of Si-O–Si groups (Fig. 1c). The FT-IR spectra of $Fe_3O_4@SiO_2-TCT-NH_2$ NPs (Fig. 1d) were characterized by the following absorption bands: stretching vibrations of C−N arising at $1257 \, cm^{-1}$, CH_2 (bending) at $1451 \, cm^{-1}$, and the C–H (symmetric and asymmetric stretching vibrations) at $2871 - 3057 \, cm^{-1}$ (Fig. 1d). As can be seen, the typical absorption peak at $3397 \, cm^{-1}$ indicated the stretching vibrations of N−H and O−H bonds (overlap) (Fig. 1d). According to Fig. 1e, the successful $Fe_3O_4@SiO_2-TCT-NH_2$ surface modification with EDTA moieties is verified. In the FT-IR spectra of $Fe_3O_4@SiO_2-EDTA$ (Fig. 1e), basic characteristic vibrations of C−H bands (asymmetric and symmetric stretching)at $2885 - 3070 \, cm^{-1}$, Si−O−Si asymmetric stretching and symmetric stretching at 1095 and $801 \, cm^{-1}$ and the stretching vibration of Fe–O were observed at $578 \, cm^{-1}$. Furthermore, the characteristic bands of the carbonyl groups were observed at $1736 \, cm^{-1}$ (C=O carboxylic acid stretching vibration) and $1629 \, cm^{-1}$ (C=O amide stretching vibration). Eventually, in terms of $Fe_3O_4@SiO_2-EDTA-Ni(II)$ (Fig. 1f), a redshift of the band at $1736 \, cm^{-1}$ is observed $(1736 \, cm^{-1} \rightarrow 1724 \, cm^{-1})$, which probably is the characteristic of carbonyl group after interaction with the nickel ions. The observed results indicate that the functional groups were successfully grafted onto the surface of the magnetic $Fe_3O_4@SiO_2$ NPs.

The crystalline structure of magnetic nanoparticles was identified with the XRD technique. As it can be found in Fig. 2a, the XRD pattern exhibited the reflection peaks at 30.1°, 35.4°, 43.1°, 53.4°, 57.0° and 62.6° that are indexed to (220), (311), (400), (422), (511) and (440) crystallographic planes of crystalline Fe_3O_4 (JCPDS 88-0866) though, the peak positions of synthesized composites remained unchanged revealing that the crystalline phases of magnetic particles is maintained after coating. These results present more evidence for the successful functionalization of nanomagnetite. However, according to Fig. 2b, c, the crystallinity of the samples decreases after the coating process. Furthermore, the XRD pattern of $Fe_3O_4@SiO_2$ shows an obvious diffusion peak at $10-20°$ because of the presence of the amorphous silica shell (Fig. 2b). In the case of $Fe_3O_4@SiO_2-EDTA-Ni(II)$ MNPs, the broad peak was transferred to lower angles due to the synergetic effect of the
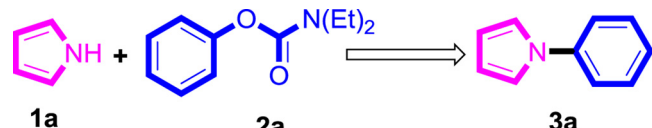
Table 3

Optimization of *N*-arylation of pyrrole with phenyl carbamates using Ni(II) catalyst.

Entry	Catalyst (mol%)	Base (equiv.)	T (°C)	Time (h)	Yield (%)[a]
1	1	NaO^{t}Bu(2.0)	100	6	91
2	1	NaOAc(2.0)	100	6	41
3	1	Na$_2$CO$_3$(2.0)	100	6	49
4	1	K$_3$PO$_4$(2.0)	100	6	72
5	1	NaOH(2.0)	100	6	51
6	1	K$_2$CO$_3$(2.0)	100	6	45
7	1	Cs$_2$CO$_3$(2.0)	100	6	78
8	1	DBU(2.0)	100	6	62
9	1	–	100	6	0
10	1	NaO^{t}Bu(1.0)	100	6	71
11	1	NaO^{t}Bu(1.5)	100	6	80
12	1	NaO^{t}Bu(2.5)	100	6	91
13	1	NaO^{t}Bu(3.0)	100	6	90
14	0.5	NaO^{t}Bu(2.0)	100	6	66
15	1.5	NaO^{t}Bu(2.0)	100	6	90
16	2	NaO^{t}Bu(2.0)	100	6	91
17	1	NaO^{t}Bu(2.0)	r.t	6	15
18	1	NaO^{t}Bu(2.0)	80	6	63
19	1	NaO^{t}Bu(2.0)	90	6	84
20	1	NaO^{t}Bu(2.0)	110	6	85
21	1	NaO^{t}Bu(2.0)	120	6	83
22	1	NaO^{t}Bu(2.0)	100	4	71
23	1	NaO^{t}Bu(2.0)	100	8	90
24	1	NaO^{t}Bu(2.0)	100	12	91

[a] Isolated yield.

Table 4

Ni catalyst effect in *N*-arylation of pyrrole with phenyl diethylcarbamate.[a]

Entry	Catalyst	Yield (%)[b]
1	Ni(acac)$_2$	0
2	NiCl$_2$	0
3	NiCl$_2$(DME)	58
4	NiBr$_2$bipy	61
5	Ni(PCy3)$_2$Cl$_2$	57
6	Ni(COD)$_2$	76
7	(dppe)Ni(*o*-tolyl)Cl	81
8	(PCy$_2$Ph)$_2$Ni(*o*-tolyl)Cl	74
9	(PCy$_3$)$_2$Ni(*o*-tolyl)Cl	79
10	EDTA-Ni(II)	82
11	Fe$_3$O$_4$@SiO$_2$-EDTA-Ni(II)	91

[a] Reaction conditions: pyrrole (1 mmol), phenyl diethylcarbamate (1 mmol), catalyst (0.018 g, 1 mol% Ni(II)), NaO^{t}Bu(2 mmol), EG (3 cm^3), 100 °C, 6 h.

[b] Isolated yield.

amorphous silica and the dendrimer (Fig. 2c). In the end, the mean diameter of nanoparticles was calculated using Scherrer's equation to be around 12 nm.

The morphology of the final magnetic nanocatalyst can be observed in TEM and FE-SEM images (Fig. 3a–c). As revealed, the magnetite nanoparticles possess uniform spherical shape (Fig. 3a, d). The TEM image of Fe$_3$O$_4$@SiO$_2$ shows the well-defined core-shell structure (Fig. 3b). Furthermore, Fig. 3c indicates the explicit structure of Fe$_3$O$_4$@SiO$_2$-EDTA-Ni(II) NPs after being coated with the organic layer. The FE-SEM photographs demonstrate that the Fe$_3$O$_4$@SiO$_2$ and Fe$_3$O$_4$@SiO$_2$-EDTA-Ni(II) NPs are almost regular spherical (Fig. 3e, f).

Moreover, these results were consistent with the particle size distribution histogram of magnetic nanoparticles, which were in a narrow distribution in the range of 8 − 16 nm, 16 − 24 nm and 23 − 37 nm and average size distribution of 12 nm, 20 nm and 31 nm for Fe$_3$O$_4$, Fe$_3$O$_4$@SiO$_2$ and Fe$_3$O$_4$@SiO$_2$-EDTA-Ni(II) NPs, respectively (Fig. 3g–i).

EDX detector coupled to the SEM was exploited to confirm the existence of nickel in the Fe$_3$O$_4$@SiO$_2$-EDTA-Ni(II) nanocatalyst (Fig. 4). Besides, the presence of C, N and O peaks along with the higher intensity of the Si peak compared with the Fe peaks indicates that the magnetite nanoparticles were trapped by silica and also, the Fe$_3$O$_4$@SiO$_2$-EDTA-Ni(II) has been successfully synthesized.
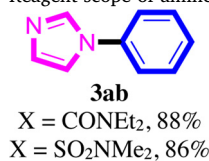
Table 5
Evaluation of various phenol derivatives as the electrophile.[a]

Entry	X	Yield (%)[b]
1	Me	10 <
2	Ac	46
3	Piv	51
4	Ms	54
5	Ts	57
6	Tf	56
7	$CO_2{}^tBu$	78
8	SO_2NEt_2	87
9	$CONEt_2$	91

[a] Reaction conditions: pyrrole(1 mmol), phenol derivatives (1 mmol), catalyst (0.018 g, 1 mol% Ni(II)), NaO^{t}Bu (2 mmol), EG (3 cm^3), 100 °C, 6 h.
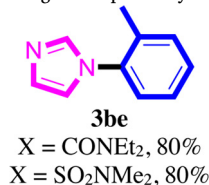[b] Isolated yield.

Table 6
Reagent scope of amines in the *N*-arylation reaction.[a]

3ab
X = $CONEt_2$, 88%
X = SO_2NMe_2, 86%

[a] Reaction conditions: phenol derivatives (1 mmol), amines (1 mmol), Ni catalyst (1 mol %, 0.018 g), NaO^{t}Bu (2 mmol), EG (3 cm^3), 100 °C, 12 h.
[b] Isolated yield.

Table 7
Reagent scope of aryl sulfamates and carbamates in the *N*-arylation reaction.[a]

3be
X = $CONEt_2$, 80%
X = SO_2NMe_2, 80%

[a]Reaction conditions: phenol derivatives (1 mmol), amines (1 mmol), Ni catalyst (1 mol %, 0.018 g), NaO^{t}Bu (2 mmol), EG (3 cm^3), 100 °C, 12 h.
[b]Isolated yield.

Thermogravimetric analysis (TGA) of the magnetic nanocatalyst was performed over the temperature range of 25−700 °C. The first weight loss for all samples are shown in Fig. 5A have been detected below 150 °C in which the adsorbed water and other solvents on the surface of the nanomaterials have been lost. The second step was observed between 150 °C and around 600 °C that shows the decomposition of coating organic layers. Moreover, a significant weight loss of nearly 42.7% in the range of 150−600 °C was obtained due to the elimination of organic material over Fe$_3$O$_4$@SiO$_2$ NPs (Fig. 5Ad).

The magnetic properties of magnetic nanostructures especially the final magnetic heterogeneous nanocatalyst was investigated using a vibrating sample magnetometer (VSM) at room temperature (Fig. 5B). The hysteresis loops of magnetite and functionalized magnetic catalyst show no elimination in magnetic properties in the loops and the remanence of superparamagnetic behavior for all samples. The magnetizations of Fe$_3$O$_4$ and Fe$_3$O$_4$@SiO$_2$-EDTA-Ni(II) MNPs were 64.8 and 28.7 emu/g, respectively (Fig. 5B). The coating with silica and the organic compounds results in a decrease in the magnetic strength of the composite. Nevertheless, Fe$_3$O$_4$@SiO$_2$-EDTA-Ni(II) possesses excellent magnetic responsibility and suitable magnetization values, which can quickly respond to the external magnetic field and disperse again after removing the external magnetic field (Fig. 5C). These results reveal that the nanocomposite exhibits good magnetic responsible as an advantage in the synthesized magnetic separable catalytic system.

The N$_2$ adsorption-desorption isotherms were conducted to investigate the porous structure and surface area of the nanoparticles. The measured specific surface areas were 480, 430.3 and 392.6 m^2/g for Fe$_3$O$_4$, Fe$_3$O$_4$@SiO$_2$ and Fe$_3$O$_4$@SiO$_2$-EDTA-Ni(II), respectively (Table 1). Also, the mean particle size of the magnetic nanocatalyst was calculated using the Scherrer equation to be 11.33, 12.64, and 14.97 nm for Fe$_3$O$_4$, Fe$_3$O$_4$@SiO$_2$, and Fe$_3$O$_4$@SiO$_2$-EDTA-Ni(II), respectively (Table 1).

Elemental analysis (EA) for Fe$_3$O$_4$@SiO$_2$-NH$_2$, Fe$_3$O$_4$@SiO$_2$-TCT, Fe$_3$O$_4$@SiO$_2$-TCT-NH$_2$ and Fe$_3$O$_4$@SiO$_2$-EDTA-Ni(II) were carried out and the data were tabulated in Table 2, which is in good agreement with the results obtained from TGA. The results displayed that the contents of C, H and N for Fe$_3$O$_4$@SiO$_2$-EDTA-Ni(II) are 21.61%, 2.87% and 9.23%, respectively.

Additionally, the loading of Ni particles on the catalyst was confirmed by the Inductively Coupled Plasma (ICP) analyzer. For this purpose, 1 g of the catalyst was stirred in HCl (37%) and then, the magnetic nanocomposite was separated by an external magnetic field. The remaining solution was analyzed by inductively coupled plasma (ICP) to determine the content of nickel. The amount of Ni on the support was determined as 0.55 mmol per gram of the catalyst.

After the preparation of the catalyst, the activity of which was investigated in the *N*-arylation of nitrogen-containing compounds. The presence of Ni(0) based catalyst is necessary in most cases to obtain the best results. In recent years, some effective achievement has been reported when Ni(I) complexes had been used for the *N*-arylation reaction in which the main challenge in developing the desired *N*-arylation reaction is using Ni(II) precatalytic moiety and difficulty reducing Ni(II) content to Ni(0). In most methodologies, some reducing agents have been applied such as Zn, Mn or triethylsilane [93–96]. It has recently been reported that even without any reducing agent for the generation of Ni(0) catalyst, the Heck and Sonogashira cross-coupling reactions proceeded well in the presence of NiCl$_2$.6H$_2$O as the catalyst and ethylene glycol as solvent [97]. This interesting result indicated that ethylene glycol could reduce the Ni(II) to the lower valent nickel species. Therefore, the *N*-arylation of pyrrole with phenyl carbamates in the presence of Ni catalyst and ethylene glycol as solvent was chosen as model reactions.

To explore an efficient catalytic system, the model reaction was investigated in detail by different parameters including the amount of catalyst, base, time and temperature to develop appropriate reaction conditions (Table 3).
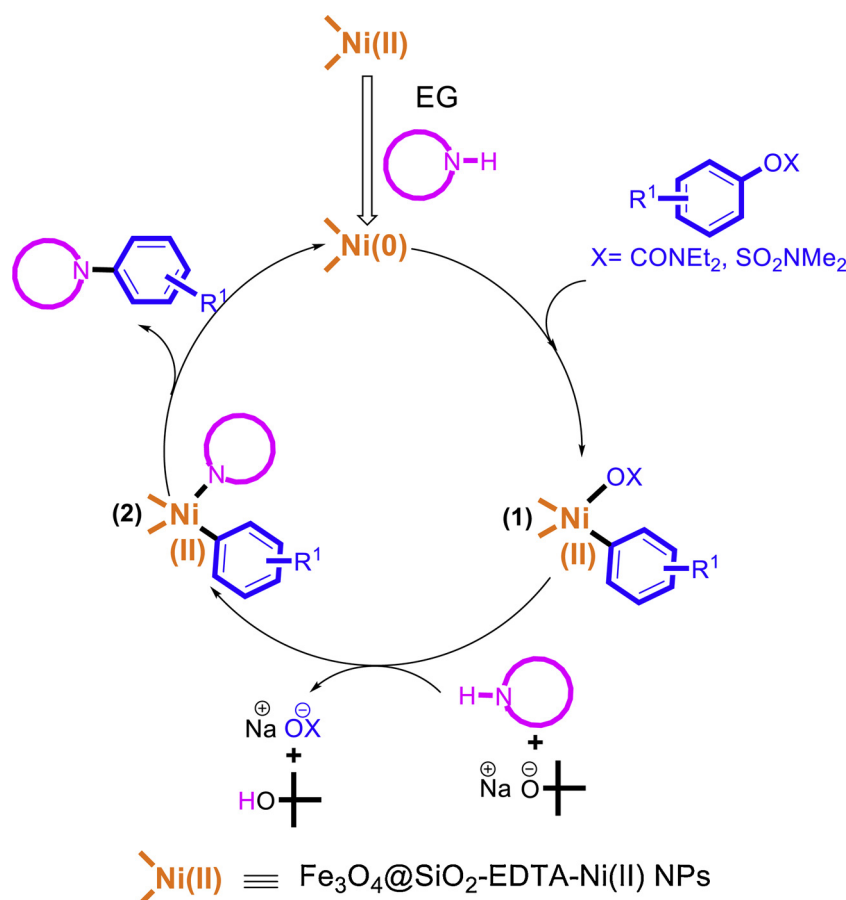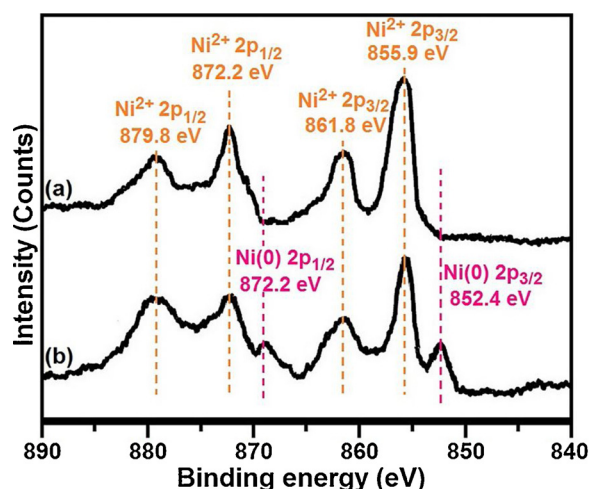
Scheme 3. A proposed catalytic cycle for the *N*-arylation reaction.

Fig. 6. XPS spectra of the (a) fresh and (b) reused catalyst.

At the outset, different bases were screened to determine their efficacy in the model reaction (Table 3, entries 1–8). These studies demonstrate that no *N*-arylation product in the absence of the base (Table 1, entry 9) and the use of sodium tert-butoxide lead to the best performance (Table 3, entry 1). Subsequently, the effect of other important factors including the amount of the catalyst and NaO^{t}Bu, time and temperature were studied in the model reaction(Table 3, entries 11–25).These investigations indicated that the highest yield of the product in the model reaction can be obtained using NaO^{t}Bu (2.0 equiv.) as a base, 0.018 g of catalyst (1 mol% Ni(II)) and EG as both solvent and reducing agent at 100 °C after 6 h (Table 3, entry 1).

With an active catalyst in hand and reliable conditions, we decided to study the application and efficiency of this Ni-based catalyst in the *N*-arylation reaction and the results summarized in Table 4. Unfortunately, the model reaction did not work with the catalysts such as Ni(acac)$_2$ and NiCl$_2$(Table 4, entries 1 and 2). When NiCl$_2$(DME), NiBr$_2$bipy and Ni(PCy$_3$)$_2$Cl$_2$ were used as the catalyst, about 70% of the desired product was observed (Table 4,entries 3–5). As expected, the model reaction catalyzed by other nickel complexes including Ni (COD)$_2$, (dppe)Ni(*o*-tolyl)Cl, (PCy2Ph)$_2$Ni(*o*-tolyl)Cl and (PCy$_3$)$_2$Ni(*o*-tolyl)Cl presented a significant increase in the yield (Table 4, entries 6–9). However, these catalysts were not as effective as Fe$_3$O$_4$@ SiO$_2$–EDTA–Ni(II) NPs (Table 4, entry 11). Even using EDTA–Ni(II) complex as homogeneous catalyst under the optimized reaction conditions, did not result in a better performance (Table 4, entry 10).

The next investigation was focused on the effect of various phenol derivatives. Hence, the most general, common and highly reactive phenol derivatives were studied in the optimal reaction conditions (Table 5). This study showed the insignificant *N*-acylation results when the anisole was used as the coupling partner (Table 5, entry1). However, the corresponding acetate, mesylate, tosylates and triflate substrates gave only modest yields of the desired product (Table 5, entries 2–6). The use of a carbonate coupling partner created the final product in good yield (Table 5, entry7). Finally, we found that the corresponding carbamate and sulfamate substrates gave the best yields of the *N*-acylation products (Table 5, entries 8 and 9). Thus, we elected these two types of electrophiles to evaluate the scope of the methodology.

After identifying the optimal conditions of the *N*-arylation reaction, we examined the scope of alkyl, aryl and heterocyclic amines using phenyl sulfamates and carbamates (Table 6). It was found that the *N*-arylation of various amines resulted good to excellent yields depending on the steric and electronic nature of the amine substrates. Heterocyclic
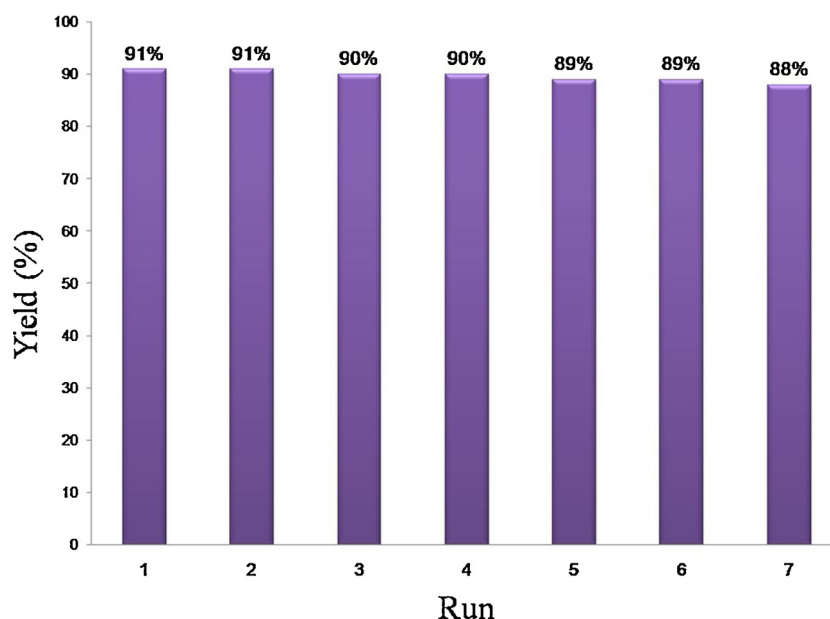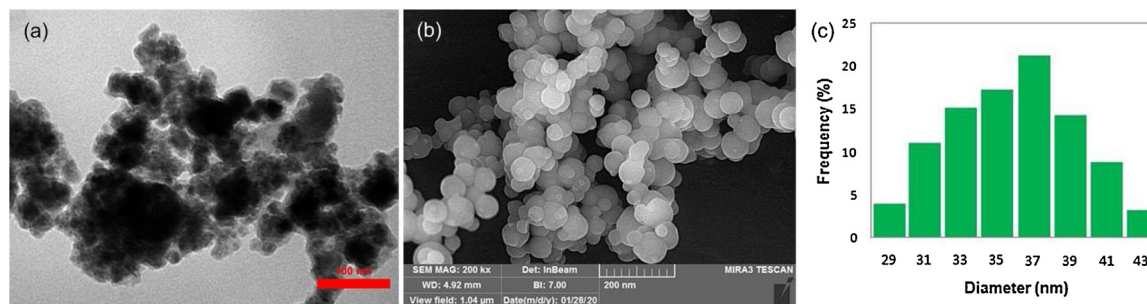
Fig. 7. Reusability of the Fe_3O_4@SiO_2-EDTA-Ni(II) NPs.

Fig. 8. TEM (a), FE-SEM (b) and DLS (c) images of Fe_3O_4@SiO_2-EDTA-Ni(II) after seventh recycling experiment.

substrates containing pyrrole, imidazole, pyrazole, indole and benzi-midazoles underwent coupling with phenyl sulfamates and carbamates under the optimized conditions and the desired products were synthe-sized in excellent yields (Table 6, entries **3aa–3af**).Aryl amines are also efficient nucleophiles in the reaction (Table 6, entries **3ag–3ai**). Aniline was also coupled in good yields (Table 6, entry **3ag**). The presence of the electron-donating groups on the phenyl ring of aniline led to the more desired product (Table 6, entry **3ah**)and the electron-withdrawing groups produced a slightly adverse influence (Table 6, entry **3ai**).Be-sides, the performance of secondary aromatic amines might be affected by steric factors. *N*-Ethylaniline as aryl amines with a little steric hin-drance reacted very well in this reaction conditions (Table 6, entry **3aj**), but diphenylamine with a high steric hindrance did not undergo into the product very effectively (Table 6, entry **3ak**).Although, the primary and secondary aliphatic amines that are the difficult class of nucleo-philic substrates in the usual *N*-arylation reactions, worked well in this optimal reaction conditions(Table 6, entries **3al–3ao**). However, sec-ondary aliphatic amines showed significantly low performances due to the steric hindrance (Table 6, entries **3an–3ao**).It should be emphasized that in the case of primary amines, good regioselectivity was observed and just the mono-aminated product was solely obtained under these reaction conditions without the formation of di-aminated product.

Furthermore, the coupling of various aryl carbamates and sulfa-mates as the electrophile with heterocyclic amines was examined under the optimal conditions (Table 7). Both aryl sulfamates and carbamates with electron-withdrawing or electron-donating substituents on the aryl ring were successfully compatible in the reaction showing the

functional group compatibility that could be coupled with heterocyclic amines to provide the products in good to excellent yields (Table 7, entries **3ba–3bq**). In addition, the sterically hindered *ortho*-substituted aryl carbamates and sulfamates reacted with various amines and pre-sented the good results (Table 7, entries **3bd–3bf** and **3bq**). It should be noted that the strong electron-withdrawing substituents such as NO_2 showed a bit better performances than other substituents in these re-action conditions (Table 7, entries **3bo–3bp**). Fortunately, the reaction showed good tolerance toward fluoride substituent and the satisfactory result was obtained (Table 7, entry **3bl**). More importantly, the het-eroaromatic substrates of carbamate and sulfamate could also partici-pate smoothly in these reaction conditions and produced the corre-sponding products in excellent yields (Table 7, entries **3bs–3bu**).

In the end, we proposed the plausible catalytic mechanism for the *N*-arylation coupling of nitrogen-containing compounds *via* C−O bond activation of aryl carbamates and sulfamates according to the reported researches in the literature, (Scheme 3) [93–97]. Initially, the process begins with the reduction of Ni(II) by nitrogen-containing compounds or ethylene glycol as the reducing agents to provide the active Ni(0) species. Subsequently, the catalytic cycle starts with the oxidative ad-dition of Ni(0) to aryl carbamates or aryl sulfamates for the *in situ* generations of the intermediate (1). This complex subsequently reacts with the nitrogen-containing compound and base (NaO^{t}Bu) to form the intermediate (2). Finally, the C−N bond formation was occurred through the reductive elimination step generates Ni(0) catalyst.

To determine the oxidation state of nickel, high resolution X-ray photoelectron spectroscopy (XPS) spectra of Ni 2p core levels were

obtained from the catalyst before and after the reaction (Fig. 6). According to the fitted data, the deconvoluted peaks at binding energy 855.9 eV and 861.8 eV are attributed to Ni $2p_{3/2}$ and peaks at 872.2 eV and 879.8 eV constitutes to Ni $2p_{1/2}$ for fresh catalyst that can be indexed to Ni^{2+} (Fig. 6a). [98] Besides, the XPS patterns of recovered catalyst show the peaks of both Ni^{2+} and Ni(0) (Fig. 6b). The peaks at around 852.4 eV and 872.2 eV were assigned to the Ni $2p_{3/2}$ and Ni $2p_{1/2}$ levels in the Ni(0) which are in good agreement with the literature report [99]. The above phenomena supported that the reaction proceeded *via* the traditional Ni^{2+}/Ni(0) cycle mechanism.

The recyclability and high stability of the economically and eco-friendly catalytic systems are so important in the industry and designing the green and effective synthetic pathways. Therefore, we focused on the investigation of stability and reusability of catalyst under the optimal reaction conditions. Therefore, the model reaction was chosen to be tested in the efficiency of catalyst behavior. After completing the model reaction, the magnetic heterogeneous catalyst was separated by using an external magnet and washed with ethanol, dried at 60 °C under vacuum and prepared for using in the next runs. As shown in Fig. 7, after seven cycles just the insignificant decrease in the catalytic activity was observed. Surprisingly, the decrease in the efficacy of catalyst after 7 runs is only 3%.

The morphology and stability of catalyst against the aggregation have been investigated after seventh run (Fig. 8). As shown in Fig. 8a and 8b, the TEM and FE-SEM images of recovered magnetic nanoparticles after the seventh cycle revealed that almost all Fe_3O_4@SiO_2-EDTA-Ni(II) particles are spherical in shape as the same as fresh catalyst indicating that the aggregation of nanoparticles is venial. Moreover, the hydrodynamic diameter of the catalyst was studied by the DLS technique (Fig. 8c) in which insignificant aggregation was observed for reused nanocatalyst and the size distribution is centered at around 37 nm.

Additionally, the catalyst was investigated by Inductively Coupled Plasma (ICP) analysis after the last run to determine the amount of nickel leaching. Accordingly, the amount of loaded nickel on the recovered catalyst was measured to be 0.54 mmol/g. Propitiously, the ICP analysis after the seventh run showed less than 1% nickel leaching. Moreover, to determine the responsibility of nickel moiety for carrying out the model reaction, the hot filtration test was performed. When the reaction time of the model reaction reached the half time of reaction quenching, the catalyst nanoparticles were taken out from the reaction mixture by an external magnetic field and the residue was allowed to be stirred under the reaction conditions. The monitoring of reaction mixture by TLC did not show any considerable progress. These results showed that only a few species of nickel may exist in the solution phase and the main responsible species that catalyzes the model reaction, is the Fe_3O_4@SiO_2-EDTA-Ni(II) nanoparticles. All of these data confirmed the high stability and reusability of the catalyst under these reaction conditions.

4. Conclusion

We have demonstrated a general, convenient and highly efficient protocol for the *N*-arylation of nitrogen-containing compounds including aliphatic and aromatic amines, indole and imidazole through C−O activation of phenol derivatives (aryl carbamates and sulfamates) in the presence of Fe_3O_4@SiO_2-EDTA-Ni(II) NPs. The main benefits of the application of phenolic derivatives in the *N*-arylation reaction are being highly rewarding because these compounds serve not only as more eco-friendly alternatives rather than aryl halides and also, they can be easily produced from cheap and available phenols. The other features of this catalytic system are the significant improvement of the substrate and functional group tolerance, high selectivity, environmentally friendly, and being economical, recoverable and reusable compared to previously published methods. Despite these unique features, this catalytic system has special applications in pharmaceutical

industries as well as in the synthesis of biologically significant compounds in which the safety, environmental and financial issues are of greater concern.

Intellectual property

We confirm that we have given due consideration to the protection of intellectual property associated with this work and that there are no impediments to publication, including the timing of publication, with respect to intellectual property. In so doing we confirm that we have followed the regulations of our institutions concerning intellectual property.

Research ethics

We further confirm that any aspect of the work covered in this manuscript that has involved human patients has been conducted with the ethical approval of all relevant bodies and that such approvals are acknowledged within the manuscript.

IRB approval was obtained (required for studies and series of 3 or more cases)

Written consent to publish potentially identifying information, such as details or the case and photographs, was obtained from the patient(s) or their legal guardian(s).

Authorship

The International Committee of Medical Journal Editors (ICMJE) recommends that authorship be based on the following four criteria:

Substantial contributions to the conception or design of the work; or the acquisition, analysis, or interpretation of data for the work; AND

Drafting the work or revising it critically for important intellectual content; AND

Final approval of the version to be published; AND

Agreement to be accountable for all aspects of the work in ensuring that questions related to the accuracy or integrity of any part of the work are appropriately investigated and resolved.

Declaration of Competing Interest

We wish to confirm that there are no known conflicts of interest associated with this publication and there has been no significant financial support for this work that could have influenced its outcome.

Appendix A. Supplementary data

Supplementary material related to this article can be found, in the online version, at doi:https://doi.org/10.1016/j.mcat.2020.110915.

References

[1] V. Nair, R.S. Menon, A.R. Sreekanth, N. Abhilash, A.T. Biju, Acc. Chem. Res. 39 (2006) 520–530.
[2] S.M. Seyed-Talebi, I. Kazeminezhad, M. Nematpour, J. Catal. 361 (2018) 339–346.
[3] L. He, F. Weniger, H. Neumann, M. Beller, Angew. Chem. Int. Ed. 55 (2016) 12582–12594.
[4] X. Yu, D. Sun, Molecules 18 (2013) 6230–6268.
[5] T. Wiglenda, R. Gust, J. Med. Chem. 50 (2007) 1475–1484.

[6] W. Deng, Y. Wang, S. Zhang, K.M. Gupta, M.J. Hülsey, H. Asakura, L. Liu, Y. Han, E.M. Karp, G.T. Beckham, P.J. Dyson, Proc. Natl. Acad. Sci. U.S.A. 115 (2018) 5093–5098.

[7] Y. Wang, S. Furukawa, S. Song, Q. He, H. Asakura, N. Yan, Angew. Chem. Int. Ed. (2019), https://doi.org/10.1002/anie.201912580.

[8] M. Carril, R. SanMartin, E. Domínguez, Chem. Soc. Rev. 37 (2008) 639–647.

[9] N.C. Bruno, M.T. Tudge, S.L. Buchwald, Chem. Sci. 4 (2013) 916–920.

[10] B. Kodicherla, M.R. Mandapati, Appl. Catal. A Gen. 483 (2014) 110–115.

[11] Y.Y. Liu, D. Liang, L.Q. Lu, W.J. Xiao, Chem. Commun. (Camb.) 55 (2019) 4853–4856.

[12] S.K. Movahed, M. Dabiri, A. Bazgir, Appl. Catal. A Gen. 481 (2014) 79–88.

[13] U.M. Gonela, S.Y. Ablordeppey, New J. Chem. 43 (2019) 2861–2864.

[14] J. Kim, J. Ok, S. Kim, W. Choi, P.H. Lee, Org. Lett. 16 (2014) 4602–4605.

[15] M. Tobisu, T. Shimasaki, N. Chatani, Angew. Chem. Int. Ed. 47 (2008) 4866–4869.

[16] T. Shimasaki, Y. Konno, M. Tobisu, N. Chatani, Org. Lett. 11 (2009) 4890–4892.

[17] M. Shigeno, K. Hayashi, K. Nozawa-Kumada, Y. Kondo, Chem. Eur. J. 25 (2019) 6077–6081.

[18] K.W. Quasdorf, X. Tian, N.K. Garg, J. Am. Chem. Soc. 130 (2008) 14422–14423.

[19] Q. Zhou, H.D. Srinivas, S. Dasgupta, M.P. Watson, J. Am. Chem. Soc. 135 (2013) 3307–3310.

[20] C.M. So, F.Y. Kwong, Chem. Soc. Rev. 40 (2011) 4963–4972.

[21] L. Zhang, J. Qing, P. Yang, J. Wu, Org.Lett. 10 (2008) 4971–4974.

[22] C.M. So, C.P. Lau, F.Y. Kwong, Angew. Chem. Int. Ed. 47 (2008) 8059–8063.

[23] P.Y. Choy, K.H. Chung, Q. Yang, C.M. So, R.W.Y. Sun, F.Y. Kwong, Chem. Asian J. 13 (2018) 2465–2474.

[24] H. Zhang, C.B. Zhou, Q.Y. Chen, J.C. Xiao, R. Hong, Org. Lett. 13 (2010) 560–563.

[25] M. McLaughlin, Org. Lett. 7 (2005) 4875–4878.

[26] T.M. Gøgsig, A.T. Lindhardt, T. Skrydstrup, Org. Lett. 11 (2009) 4886–4888.

[27] T. Agrawal, S.P. Cook, Org. Lett. 15 (2012) 96–99.

[28] P. Leowanawat, N. Zhang, A.M. Resmerita, B.M. Rosen, V. Percec, J. Org, Chem. 76 (2011) 9946–9955.

[29] G.J. Chen, F.S. Han, Eur. J. Org. Chem. 2012 (2012) 3575–3579.

[30] J.Y. Yu, R. Kuwano, Org. Lett. 10 (2008) 973–976.

[31] C. Li, J. Xing, J. Zhao, P. Huynh, W. Zhang, P. Jiang, Y.J. Zhang, Org. Lett. 14 (2011) 390–393.

[32] I. Dindarloo Inaloo, S. Majnooni, Chem. Select. 4 (2019) 7811–7817.

[33] T. Mesganaw, A.L. Silberstein, S.D. Ramgren, N.F.F. Nathel, X. Hong, P. Liu, N.K. Garg, Chem. Sci. 2 (2011) 1766–1771.

[34] W.J. Shi, H.W. Zhao, Y. Wang, Z. C.Cao, L.S. Zhang, D.G. Yu, Z.J. Shi, Adv. Synth. Catal. 358 (2016) 2410–2416.

[35] I.D. Inaloo, S. Majnooni, New J. Chem. 43 (2019) 11275–11281.

[36] Y. Wang, S. Furukawa, X. Fu, N. Yan, ACS Catal. 10 (2019) 311–335.

[37] K.W. Quasdorf, M. Riener, K.V. Petrova, N.K. Garg, J. Am. Chem. Soc. 131 (2009) 17748–17749.

[38] A.R. Sardarian, I.D. Inaloo, RSC Adv. 5 (2015) 76626–76641.

[39] A.R. Modarresi-Alam, I.D. Inaloo, E. Kleinpeter, J. Mol. Struct. 1024 (2012) 156–162.

[40] I.D. Inaloo, S. Majnooni, Chem. Select. 3 (2018) 4095–4100.

[41] A.R. Sardarian, I.D. Inaloo, A. R.Modarresi-Alam, Mol. Divers 22 (2018) 863–878.

[42] R.A.A. Abdine, G. Kurpik, A. Walczak, S.A.A. Aeash, A.R. Stefankiewicz, F. Monnier, M. Taillefer, J. Catal. 376 (2019) 119–122.

[43] Y. Han, M. Zhang, Y.Q. Zhang, Z.H. Zhang, Green Chem. 20 (2018) 4891–4900.

[44] Z. Huang, F. Li, B. Chen, F. Xue, G. Chen, G. Yuan, Appl. Catal. A Gen. 403 (2011) 104–111.

[45] H. Li, J. Bai, J. Wang, C. Li, Mol. Catal. 431 (2017) 49–56.

[46] S.G. Rull, R.J. Rama, E. Álvarez, M.R. Fructos, T.R. Belderrain, M.C. Nicasio, Dalton Trans. 46 (2017) 7603–7611.

[47] R.T. McGuire, J.F. Paffile, Y. Zhou, M. Stradiotto, ACS Catal. 9 (2019) 9292–9297.

[48] A.M. Fiore, G. Romanazzi, M.M. Dell'Anna, M. Latronico, C. Leonelli, M. Mali, A. Rizzuti, P. Mastrorilli, Mol. Catal. 476 (2019) 110507–110516.

[49] T.J. Barker, E.R. Jarvo, J. Am. Chem. Soc. 131 (2009) 15598–15599.

[50] S.Z. Tasker, E.A. Standley, T.F. Jamison, Nature 509 (2014) 299–309.

[51] S. Luo, D.G. Yu, R.Y. Zhu, X. Wang, L. Wang, Z.J. Shi, Chem. Commun. (Camb.) 49 (2013) 7794–7796.

[52] T. Mesganaw, N.K. Garg, Org. Process Res. Dev. 17 (2013) 29–39.

[53] K. Hattori, A. Ziadi, K. Itami, J. Yamaguchi, Chem. Commun. (Camb.) 50 (2014) 4105–4107.

[54] Z. Ruan, N. Sauermann, E. Manoni, L. Ackermann, Angew. Chem. Int. Ed. 56 (2017) 3172–3176.

[55] M. Peña-López, P. Piehl, S. Elangovan, H. Neumann, M. Beller, Angew. Chem. Int. Ed. 55 (2016) 14967–14971.

[56] S. C.Chen, F.Tian N.Li, N. N.Chai, M.Y. He, Q. Chen, Mol. Catal. 450 (2018) 104–111.

[57] G. Toma, K.I. Fujita, R. Yamaguchi, Eur. J. Org. Chem. 2009 (2009) 4586–4588.

[58] J.P. Wolfe, S.L. Buchwald, J. Am. Chem. Soc. 119 (1997) 6054–6058.

[59] A.V. Gatien, C.M. Lavoie, R.N. Bennett, M.J. Ferguson, R. McDonald, E.R. Johnson, A.W. Speed, M. Stradiotto, ACS Catal. 8 (2018) 5328–5339.

[60] C.M. Lavoie, M. Stradiotto, Bisphosphines: ACS Catal. 8 (2018) 7228–7250.

[61] T. Morioka, S. Nakatani, Y. Sakamoto, T. Kodama, S. Ogoshi, N. Chatani, M. Tobisu, Chem. Sci. 10 (2019) 6666–6671.

[62] M. Marin, R.J. Rama, M.C. Nicasio, Chem. Rec. 16 (2016) 1819–1832.

[63] B. Su, Z.C. Cao, Z.J. Shi, Acc. Chem. Res. 48 (2015) 886–896.

[64] C. Bolm, J.P. Hildebrand, J. Rudolph, Synthesis 2000 (2000) 911–913.

[65] A. Nishizawa, T. Takahira, K. Yasui, H. Fujimoto, T. Iwai, M. Sawamura, N. Chatani, M. Tobisu, J. Am. Chem. Soc. 141 (2019) 7261–7265.

[66] N. Iranpoor, F. Panahi, Adv. Synth. Catal. 356 (2014) 3067–3073.

[67] N.H. Park, G. Teverovskiy, S.L. Buchwald, Org. Lett. 16 (2013) 220–223.

[68] T. Shimasaki, M. Tobisu, N. Chatani, Angew. Chem. Int. Ed. 49 (2010) 2929–2932.

[69] F. Strieth-Kalthoff, A.R. Longstreet, J.M. Weber, T.F. Jamison, ChemCatChem 10 (2018) 2873–2877.

[70] L. Ackermann, R. Sandmann, W. Song, Org. Lett. 13 (2011) 1784–1786.

[71] M. Tobisu, N. Chatani, Acc. Chem. Res. 48 (2015) 1717–1726.

[72] P. Alvarez-Bercedo, R. Martin, J. Am. Chem. Soc. 132 (2010) 17352–17353.

[73] A.S. Chouhan, A.K. Sarma, Renewable Sustainable Energy Rev. 15 (2011) 4378–4399.

[74] I.D. Inaloo, S. Majnooni, New J. Chem. 42 (2018) 13249–13255.

[75] A.R. Sardarian, I. Dindarloo Inaloo, A.R. Modarresi-Alam, E. Kleinpeter, U. Schilde, J. Org. Chem. 84 (2019) 1748–1756.

[76] A.H. Lu, E.E. Salabas, F. Schüth, Angew. Chem. Int. Ed. 46 (2007) 1222–1244.

[77] L.M. Rossi, N.J. Costa, F.P. Silva, R. Wojcieszak, Green Chem. 16 (2014) 2906–2933.

[78] J. Govan, Y.K. Gun'ko, Nanomaterials 4 (2014) 222–241.

[79] R. Hudson, Y. Feng, R.S. Varma, A. Moores, Green Chem. 16 (2014) 4493–4505.

[80] Y. Zhu, L.P. Stubbs, F. Ho, R. Liu, C.P. Ship, J.A. Maguire, N.S. Hosmane, ChemCatChem. 2 (2010) 365–374.

[81] M. Neamtu, C. Nadejde, V.D. Hodoroaba, R.J. Schneider, L. Verestiuc, U. Panne, Sci. Rep. 8 (2018) 6278.

[82] M.B. Gawande, P.S. Branco, R.S. Varma, Chem. Soc. Rev. 42 (2013) 3371–3393.

[83] I.D. Inaloo, S. Majnooni, M. Esmaeilpour, Eur. J. Org. Chem. 2018 (2018) 3481–3488.

[84] M.B. Gawande, Y. Monga, R. Zboril, R.K. Sharma, Coord. Chem. Rev. 288 (2015) 118–143.

[85] D.K. Yi, S.T. Selvan, S.S. Lee, G.C. Papaefthymiou, D. Kundaliya, J.Y. Ying, J. Am. Chem. Soc. 127 (2005) 4990–4991.

[86] K. Khoshnevisan, F. Vakhshiteh, M. Barkhi, H. Baharifar, E. Poor-Akbar, N. Zari, H. Stamatis, A.K. Bordbar, Mol. Catal. 442 (2017) 66–73.

[87] H.L. Ding, Y.X. Zhang, S. Wang, J.M. Xu, S.C. Xu, G.H. Li, Chem. Mater. 24 (2012) 4572–4580.

[88] A.R. Sardarian, M. Zangiabadi, I.D. Inaloo, RSC Adv. 6 (2016) 92057–92064.

[89] A.R. Sardarian, I. DindarlooInaloo, M. Zangiabadi, Catal. Lett. 148 (2018) 642–652.

[90] A.R. Sardarian, I.D. Inaloo, M. Zangiabadi, New J. Chem. 43 (2019) 8557–8565.

[91] I.D. Inaloo, S. Majnooni, Eur. J. Org. Chem. 2019 (2019) 6359–6368.

[92] H. Zeng, Z. Qiu, A. Dominguez-Huerta, Z. Hearne, Z. Chen, C.J. Li, ACS Catal. 7 (2016) 510–519.

[93] C. Chen, L.M. Yang, J. Org. Chem. 72 (2007) 6324–6327.

[94] J.H. Huang, L.M. Yang, Org.Lett. 13 (2011) 3750–3753.

[95] C. Desmarets, R. Schneider, Y. Fort, J. Org. Chem. 67 (2002) 3029–3036.

[96] N. Nowrouzi, M. Zarei, Tetrahedron 71 (2015) 7847–7852.

[97] S. Adhikari, G. Madras, Phys. Chem. Chem. Phys. 19 (2017) 13895–13908.

[98] T.Y. Yung, L.Y. Huang, T.Y. Chan, K.S. Wang, T.Y. Liu, P.T. Chen, C.Y. Chao, L.K. Liu, Nanosc. Res. Lett. 9 (2014) 444.